Available online at www.sciencedirect.com
SCIENCE DIRECT®
Thin Solid Films 425 (2003) 175–184
thin solid films
www.elsevier.com/locate/tsf

The effect of annealing conditions on the red photoluminescence of nanocrystalline Si/SiO_2 films

Xiaochun Wu[a,*], Alpan Bek[a], Alexander M. Bittner[a], Ch. Eggs[b], Ch. Ossadnik[b], S. Veprek[b]

[a]*Max-Planck Institut fuer Festkoerperforschung, Heisenbergstrasse 1, D-70569 Stuttgart, Germany*
[b]*Institut fuer Chemie Anorganischer Materialien, Technische Universitaet Muenchen, Lichtenbergstr. 4, D-85747 Garching, Germany*

Received 18 June 2002; received in revised form 24 October 2002; accepted 12 November 2002

Abstract

Nanocrystalline Si (nc-Si) embedded in a SiO_2 matrix, fabricated by plasma CVD and a subsequent post-treatment shows a broad red photoluminescence (PL). In this paper, the effects of annealing temperature, atmosphere and time on the red PL from 1.75 to 1.5 eV have been investigated in detail. It is found that the spectral shift and the PL intensity from 1.75 to 1.5 eV show a strong and unique dependence on annealing conditions. For a PL approximately 1.75 eV, upon 400 °C forming gas annealing, the spectral shift and the peak intensity versus accumulation annealing times show a novel temporal oscillation. This unique dependence and the novel temporal oscillation behavior, which have not been reported in porous silicon, exclude nc-Si itself as the source of the red PL. Instead they favor oxygen thermal donors (TDs)-like defect states as PL centers. This is in consensus with our earlier results of defect studies using electron spin resonance in this system. Furthermore, two PL centers in this red PL were distinguished according to their variance in annealing temperature- and time-dependence. The spectral change between 1.5 and 1.75 eV upon annealing conditions can be qualitatively explained by using the formation and annihilation kinetics of two oxygen TDs-like defect state.

Keywords: Photoluminescence; Thermal donors; Annealing conditions

1. Introduction

Since the discovery of a strong visible photoluminescence (PL) in porous silicon (PS) in 1990 [1], many experiments have been carried out in the hope of a potential application of Si in optoelectronic devices. Although a large volume of experimental data is available in the literature, a detailed understanding of the PL mechanism has not been achieved yet [2,3]. So far, mainly two models are proposed to interpret the origin of the visible PL: (1) pure quantum size effect (QSE) [4] and (2) surface state model [5]. As is well-known, for PL phenomena, two important processes are the formation of photoexcited carriers (excitation process) and the radiative recombination of the photoexcited carriers through PL centers (luminescence process). For the pure QSE, it is considered that both the excitation process and the PL process originate from nanocrystalline Si (nc-Si). For the surface state model, it is considered that the excitation process originates from nc-Si and the PL process originates from a special surface state. As for the surface state model, various surface species such as siloxene [6], polysilanes [7], SiH_2 [8], Si band-tail states [9], interfacial oxide-related defect centers [2], nonbridging oxygen hole centers [10], and oxyhydride-like emitters [11] have been suggested as the source of the visible PL. Among them, interfacial oxide-related defect centers are widely accepted, but still the detailed structures of these centers are unclear [2,10–17]. Gole et al. even suggested a third model; i.e. both the light excitation process and the PL process are due to a surface-bound silanone-based silicon oxyhydride fluorophor, based on their investigations on the origin of the PL in PS [11–13]. Recently, studies from Wolkin et al. seemed to clarify some disputes among the source of visible PL in PS [18]. They pointed out that depending on the size of PS and on the interfacial chemical

*Corresponding author. Tel.: +49-711-689-1432; fax: +49-711-689-1709.
E-mail address: x.wu@fkf.mpg.de (X. Wu).

0040-6090/03/$ - see front matter © 2002 Elsevier Science B.V. All rights reserved.
PII: S0040-6090(02)01113-6

environment, either PS itself or the Si=O surface state can be the source of the visible PL.

In addition to the studies of the visible PL in PS produced by the wet electrochemical method, studies of nc-Si fabricated by various dry chemical techniques have also been carried out in order to understand the PL mechanism [19–21]. Veprek and Wirschem have reported the red PL approximately 1.5 eV in nc-Si/SiO_2 films produced by plasma CVD and subsequent post-treatment in detail before. Thereby, oxide-related defect states were suggested to be the possible source of this red PL [22]. Later, defect studies using electron spin resonance (ESR) technique in this system further showed the correlation of the integrated PL intensity with the concentration of oxygen thermal donors (TDs)-related defect states, indicating that this kind of oxygen-related defect was responsible for the observed red PL in this system [23].

In the present study, we further extend our investigations to the effects of annealing temperature, atmosphere, and time on the spectral change of the red PL because the formation and annihilation kinetics of oxygen TDs in bulk crystalline Si is both annealing temperature- and time-dependent. A strong and unique dependence of the red PL on annealing conditions has been observed between 1.75 and 1.5 eV. For a PL approximately 1.75 eV, upon 400 °C forming gas annealing, the spectral shift and the peak intensity versus annealing times show a novel temporal oscillation. This unique dependence and the novel temporal oscillation behavior exclude nc-Si itself as the source of the red PL. Instead they favor oxygen TDs-like defect states as PL centers. Furthermore, two PL centers in this red PL were distinguished according to their variance in annealing temperature- and time-dependence. The spectral change between 1.5 and 1.75 eV upon annealing conditions can be qualitatively explained by using the formation and annihilation kinetics of two oxygen TDs (Si NL8 and Si NL10)-like defect state.

2. Experiment

The detailed synthesis of Si nanocrystallites by plasma CVD and post-treatment has been reported previously [22]. The typical preparation of a sample is as follows: first, an amorphous Si film is deposited onto a Si (1 0 0) wafer from a pure silane plasma. The film is annealed under 0.03 mbar of hydrogen flow at 660 °C for 40 min afterwards to decrease the amount of hydrogen. Then the film is pre-oxidized under a flow of pure oxygen at 350 °C for a chosen time in order to allow oxygen to diffuse into the film. Finally, the pre-oxidized film is annealed at high temperature in a forming gas (FG, 5 mol.% hydrogen in nitrogen) atmosphere for a chosen time in order to obtain Si nanocrystallites surrounded by a SiO_2 matrix and to obtain a red PL. Crystallite size

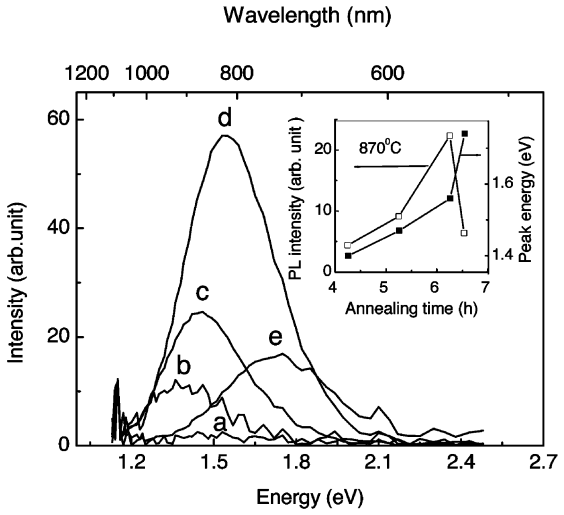

Fig. 1. Evolution of PL Spectra after 870 °C FG annealing of (a) 15 min; (b) 4 h 15 min; (c) 5 h 15 min; (d) 6 h 15 min; and (e) 6 h 32 min. *Inset*: the integrated PL intensity and the peak energy vs. annealing time.

and the fraction of nc-Si in the film are controlled by FG annealing time. The nc-Si/SiO_2 film was characterized with X-ray diffraction (XRD, Siemens Diffractometer D5000). The excitation source for room temperature steady-state PL spectra was the 325 nm line of a He–Cd laser (Omnichrome Series 56). The maximum pump power density of the laser was 0.4 W/cm^2. PL signals were spectrally resolved with a grating spectrometer (Spex Model 1681B) and detected by a Si diode in the lock-in mode. The calibration of the spectral sensitivity of the whole measuring system was performed using a tungsten standard lamp.

3. Results

3.1. Appearance and spectral changes of the PL upon high temperature annealing

As mentioned in the preparation procedure section, the red PL from a nc-Si/SiO_2 film could be observed only after several hours of high temperature FG annealing. One example was given in Fig. 1. After 4 h under high temperature annealing at 870 °C, the red PL appears. Its intensity increases upon further annealing, accompanying a blueshift of the peak energy. After certain times, the intensity decreases with further annealing and the peak energy blueshifts to approximately 1.75 eV. The dependence of the integrated PL intensity and the spectral shift on annealing times is given in Fig. 1 inset. It shows a dominant PL approximately 1.5 eV. Fig. 2 presents the corresponding variations in the XRD diagram. Increasing annealing times, due to the oxidation of nc-Si by the oxygen adsorbed in the film in the previous step, the amount of nc-Si in the film decreases,

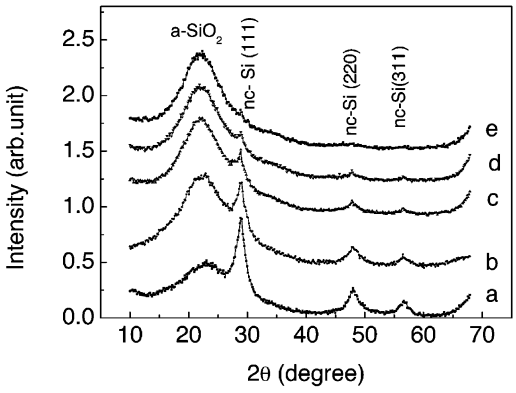

Fig. 2. The XRD diagrams after 870 °C FG annealing of (a) 15 min; (b) 4 h 15 min; (c) 5 h 15 min; (d) 6 h 15 min; and (e) 6 h 32 min, showing the change in size and amount of nc-Si in the film.

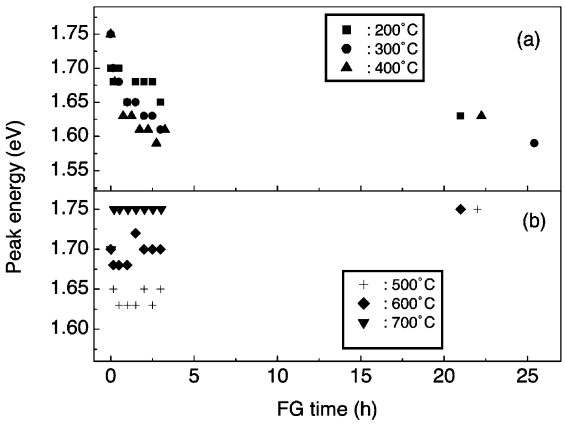

Fig. 3. The peak energy as a function of FG annealing times at annealing temperatures of (a) 200, 300 and 400 °C and of (b) 500, 600 and 700 °C.

accompanying an obvious increase in the amount of amorphous SiO_2. Generally, the effect of high temperature FG annealing can be divided into three stages [24]. In the first stage, the PL intensity from the nc-Si/SiO_2 film increases, and the peak energy shows a blueshift from 1.3 to 1.55 eV (Fig. 1b–d). During this stage, the concentration of nc-Si in the film decreases appreciably and the average dimension of nc-Si also decreases from approximately 30 to 15 Å evaluated using Scherra's formula for the XRD measurements (Fig. 2b–d). In addition, due to the rapid high temperature oxidation, the color of the film changes from brown to gray. In the second stage, the PL intensity further increases, while the peak energy does not show any obvious change. In Fig. 1, we do not see the second stage, but it has been observed in many other samples and studied in detail by Veprek and Wirschem [22]. At this stage, the nc-Si/SiO_2 film shows a strong red PL. The peak energy is 1.55 ± 0.05 eV, determined by the detailed preparation conditions of the film. At this stage, the correlation between the PL intensity and the oxygen TDs concentration from ESR measurements has been demonstrated [23]. In the third stage, the PL intensity decreases, and the peak energy blueshifts from 1.55 to approximately 1.75 eV (Fig. 1d–e). During the second and third stage, the film color shows no observable change. Due to the variance in the detailed synthesis parameters for the films, the time range required for the different stages in different films is also different, though the change trend of the red PL is similar.

Above we give a general description of the three stages of the red PL from nc-Si/SiO_2 films. Since the first (1.3–1.55 eV) and the second stages ($\approx$1.55 eV) have been reported in detail elsewhere [22,24], we will report here the effects of annealing conditions on the PL approximately 1.75 eV (in the third stage).

3.2. The influence of FG annealing temperatures on the PL approximately 1.75 eV

It was found that the PL approximately 1.75 eV shows interesting dependence on annealing conditions. Fig. 3 gives the shift of the peak energy vs. annealing times at different FG annealing temperatures for one sample. For clarity, the effect of annealing temperatures at 200, 300 and 400 °C is shown in Fig. 3a, while that at 500, 600 and 700 °C is presented in Fig. 3b. Fig. 4 gives the corresponding PL intensity change, with the intensity normalized to that of the starting position. For each temperature curve, this starting point was obtained by annealing the film at 700 °C for several minutes. Below 400 °C annealing, the peak energy redshifts and the PL intensity increases with increasing annealing times. The lower the temperature, the slower the redshift and the increase in intensity. Above 400 °C annealing

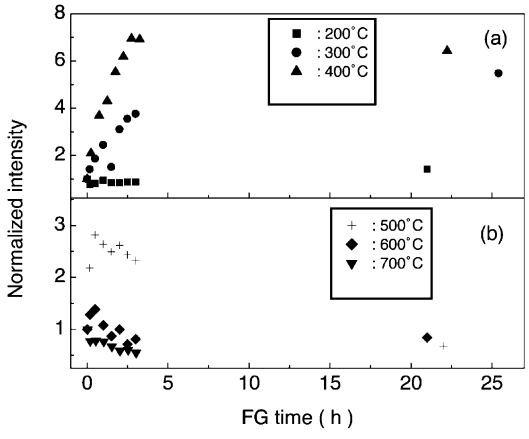

Fig. 4. The normalized PL intensity as a function of FG annealing times at annealing temperatures of (a) 200, 300 and 400 °C and of (b) 500, 600 and 700 °C.

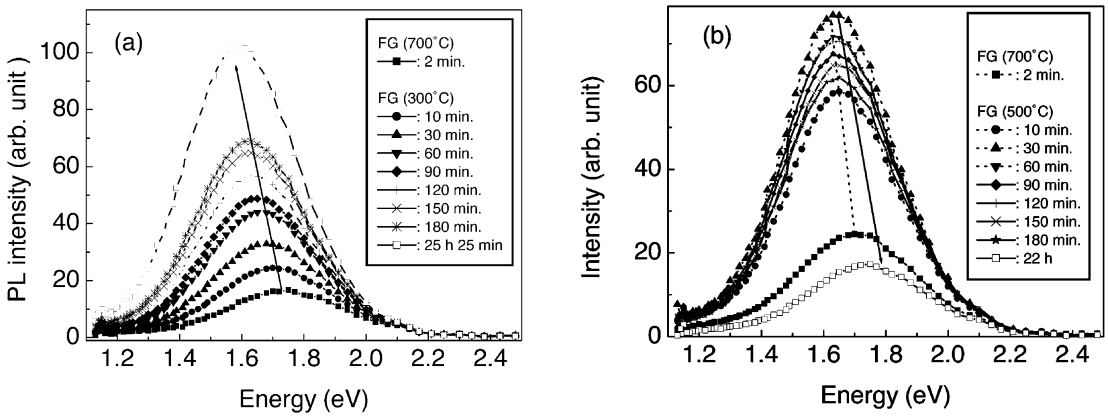

Fig. 5. PL spectra measured after different annealing times at annealing temperatures of (a) 300 °C and (b) 500 °C. Lines with arrow indicate the direction of spectra variation.

(500 and 600 °C), the peak energy first redshifts and the PL intensity increases; a blueshift up to approximately 1.75 eV and intensity decrease follows. At 700 °C annealing for a short time, the peak energy remains unchanged, and the PL intensity shows a small decrease. Therefore, for the PL approximately 1.75 eV, FG annealing at lower temperatures ($\leqslant$400 °C) leads to an increase in PL intensity and to a redshift in peak energy. FG annealing at intermediate temperatures (400 °C$\leqslant T<$700 °C) results in an increase in intensity and a redshift in peak energy for short annealing times, but a decrease in intensity and a blueshift in peak energy for long annealing times. Short time FG annealing at high temperatures ($\approx$700 °C) causes no appreciable effect. This indicates that the spectral shift and the intensity variation of the PL are both temperature- and time-dependent. Fig. 5a and b depicts the evolutions of PL spectra at different annealing times for annealing temperatures 300 and 500 °C, respectively. It can be seen that for the anneal at 300 °C, during the whole annealing process (25 h 25 min), the PL gradually redshifts from 1.75 to 1.59 eV and its intensity also gradually increases. In the case of 500 °C annealing, the PL redshifts from 1.70 to 1.63 eV during the first 60 min annealing and the PL intensity reaches its maximum, then the PL gradually blueshifts from 1.63 to 1.75 eV and its intensity correspondingly decreases from 60 min to 22 h. The redshift of the peak energy at 500 °C is smaller than that at 300 °C. Therefore, both annealing temperature and annealing time determine the magnitude of the spectral shift and of the intensity change.

In addition, a general trend is that PL intensity decreases (increases) with a blueshift (redshift) of the peak energy at all annealing temperatures. Fig. 6 demonstrates this correlation between the integrated intensity and the peak energy using data from 200 to 700 °C (i.e. data from Figs. 3 and 4). In Fig. 6, instead of annealing time, the peak energy is chosen as x-axis. The integrated PL intensity at each annealing time vs. the corresponding peak energy at the same annealing time is shown. Data from different annealing temperatures (from 200 to 700 °C) are given in different symbols. From Figs. 3–6, we can see that the PL can be tuned continuously between 1.5 and 1.75 eV through the control of the annealing conditions. But the final peak energy of the PL at each annealing temperature is either approximately 1.75 eV (500, 600 and 700 °C annealing) or approximately 1.5 eV (300 and 400 °C annealing) for the annealing times we used. The PL approximately 1.75 eV exhibits itself better after annealing at higher temperatures for a shorter time ($\geqslant$700 °C) or at intermediate temperatures (400–600 °C) for a longer time while the PL approximately 1.5 eV exhibits itself better after annealing at lower temperatures for a longer time ($<$400 °C) or at intermediate temperatures for a shorter time (400–600 °C). The former is thermodynamically more stable than the latter. This suggests that there exist at least two luminescent states with different stabilities in annealing

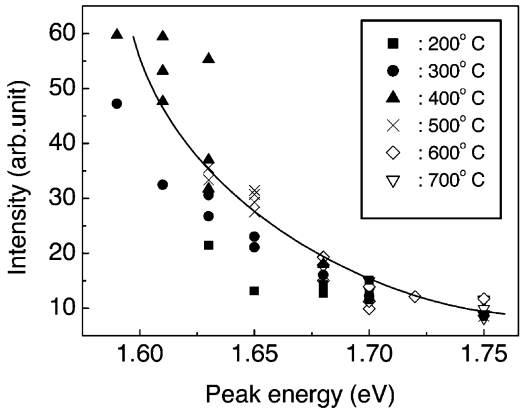

Fig. 6. Correlation between the peak energy and the PL intensity under FG atmosphere for one sample at different annealing temperatures. The solid line is a guide to the eye.

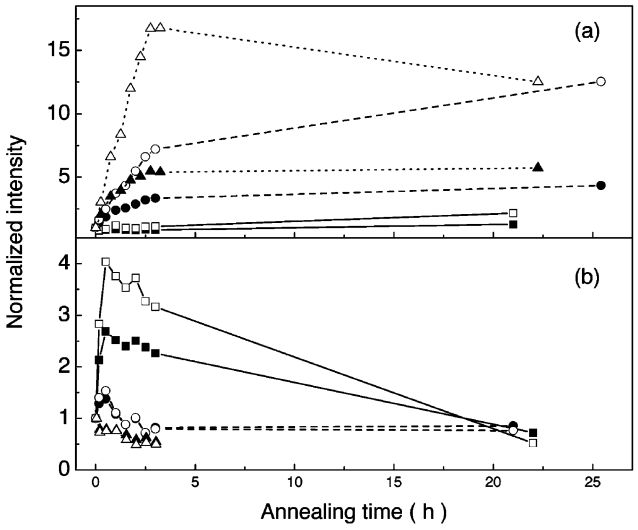

Fig. 7. The PL intensities at 1.75 and 1.46 eV vs. annealing times at different temperatures with solid-square + solid line, solid-circle + dash line and solid-triangle + dot line representing 1.75 eV at 200, 300 and 400 °C, respectively in (a) and at 500, 600 and 700 °C, respectively in (b) and with open-square + solid line, open-circle + dash line and open-triangle + dot line denoting 1.46 eV at 200, 300 and 400 °C, respectively in (a) and at 500, 600 and 700 °C, respectively in (b).

temperatures and times. One is located at a lower energy (≈1.5 eV) with a lower thermal stability while the other is located at a higher energy with a higher thermal stability (≈1.75 eV). The spectral changes from 1.75 to 1.5 eV upon annealing can be explained in the following two ways: (1) the 1.75 eV PL centers gradually change to the 1.5 eV PL centers upon annealing; therefore PL gradually redshifts from 1.75 to 1.5 eV. In this way, we will observe an increase in the PL intensity approximately 1.5 eV and a decrease in the PL intensity approximately 1.75 eV. (2) These two PL centers do not change to each other upon annealing. They just have different formation and decay kinetics. If the 1.5 eV PL centers grow much faster than the 1.75 eV PL centers or if the 1.5 eV PL centers form while the 1.75 eV PL centers decay (but do not change to 1.5 eV PL centers), the whole PL will also redshift. From Fig. 5, we can see that with increasing annealing time (<60 min), the PL intensities at 1.75 and 1.5 eV both increase. To see this more clearly, we further show the normalized PL intensities at 1.75 and 1.46 eV (a little redshift from 1.5 eV for the better avoidance of a possible overlap of the two bands) vs. annealing times at different annealing temperatures in Fig. 7. For 300, 400 and 500 °C annealing, we can see clearly that during the redshift of the peak energy (Fig. 3), the PL intensities at 1.75 and 1.46 eV both increase with increasing annealing times, but the increase rate of PL intensity at 1.46 eV is much larger than that at 1.75 eV. This means that the redshift of the PL from 1.75 to 1.5 eV is not caused by the transformation between these two PL centers, but is due to the difference in their growth rates. The blueshift of the PL can be explained using their difference in decay rates. In Fig. 7b for the case of 500 °C annealing, we can see clearly that during the blueshift of the peak energy, the decay rate of PL intensity at 1.46 eV is faster than that at 1.75 eV. This leads to the blueshift of the peak energy. On the other hand, slower decay rate for 1.75 eV PL also means that it is thermodynamically more stable than 1.5 eV PL. This agrees with the experimental results. In addition, the redshift of peak energy via annealing times always accompanies with an increase in PL intensity while the blueshift of peak energy accompanies with a decrease in PL intensity. This means that with the redshift of the peak energy we have a dominant growth process for both PL centers while with the blueshift of the peak energy we have a dominant decay process for them.

3.3. The effect of annealing atmosphere

It is well known that hydrogen plays an important role in the PL process for PS. The roles of hydrogen that have been suggested are: (1) the passivation of dangling bonds [25–27]; (2) as one of the components of the luminescence centers [11,29]; and (3) responsible for the change of the interfacial environment around Si crystallites by adsorption and desorption processes [11,29].

In order to determine the role of hydrogen in our case, the annealing atmosphere was changed from FG to oxygen. Fig. 8 compares the effect of annealing atmospheres on the red PL. The PL shows similar redshifts for both atmospheres (Fig. 8a), indicating that annealing atmospheres have no direct correlation to the redshift. This further verifies that the redshift corre-

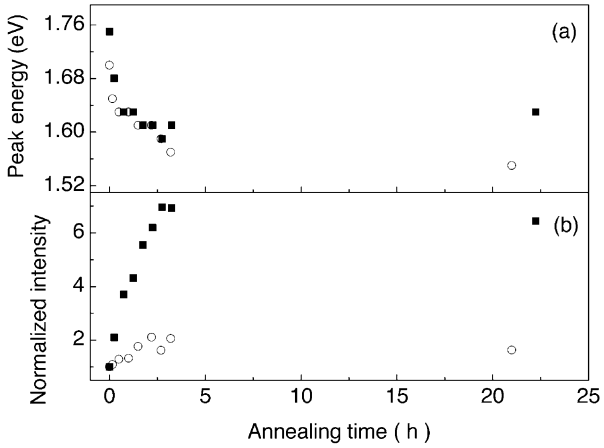

Fig. 8. The peak energy (a) and the PL intensity (b) versus annealing times upon 400 °C annealing in an oxygen (open circle) atmosphere and in a FG atmosphere (solid square).

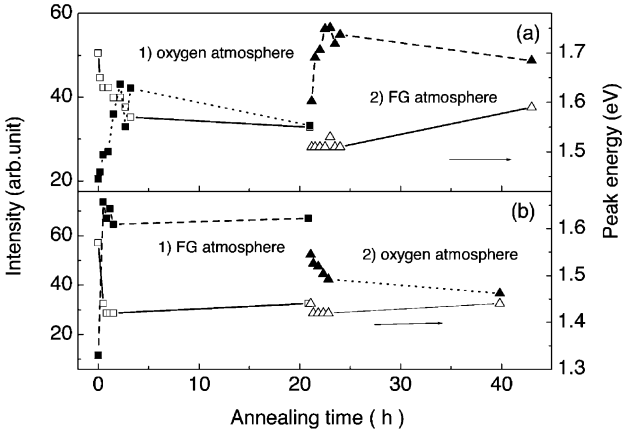

Fig. 9. The dependence of the peak energy and the PL intensity on annealing times at 400 °C with (a) first oxygen annealing, then FG annealing and with (b) first FG annealing, then oxygen annealing. Open square and triangle for the peak energy and solid square and triangle for the PL intensity.

sponds to the growth process of PL centers. The increase in PL intensity for the FG atmosphere is however much larger than that for the oxygen atmosphere (Fig. 8b), indicating that hydrogen is a much effective passivation gas to nonradiative combination centers than oxygen. In order to further distinguish the role of annealing atmospheres, we use a two-step annealing procedure to separate the growth process of PL centers and the passivation process of nonradiative centers. As shown in Fig. 9a, the peak energy monotonically decreases with the annealing time by a first oxygen annealing, which indicates the growth process of PL centers, a subsequent FG anneal causes a very small redshift in peak energy but a strong enhancement in PL intensity after a short time annealing. This strongly supports the passivation role of hydrogen to nonradiative centers. Fig. 9b presents a reverse annealing order for another sample. After the redshift in peak energy reaches its maximum by the first FG annealing, the subsequent oxygen anneal reduces the PL intensity accompanying with a very small redshift in peak energy after short time annealing. This indicates that instead of passivation of nonradiative centers oxygen annealing increases their concentrations. Since the redshifts vs. annealing times match quite well after short time annealing under both atmospheres, we assume that annealing atmospheres do not influence the growth process of PL centers, i.e. similar amount of PL centers for both annealing atmospheres at same annealing times. However, FG atmosphere reduces the amount of nonradiative centers while oxygen atmosphere increases their amount. The actual PL is determined by both the concentrations of PL centers and of nonradiative recombination centers. This leads to the much strong enhancement of PL in the case of FG annealing (Fig. 8b). Therefore, the main role of hydrogen here is the effective passivation of nonradiative recombination centers.

3.4. The effect of annealing times upon 400 °C annealing

At an annealing temperature of 400 °C, longer time annealing ($\geqslant$10 h) also results in a blueshift of the PL and in a decrease of its intensity (Figs. 8 and 9). Fig. 10 depicts the dependence of the intensity and the peak energy on annealing times upon 400 °C. At shorter annealing times ($<$10 h), the PL redshifts from 1.68 to 1.51 eV, accompanying an increase in the intensity. With the prolongation of the annealing time (from 10 to 70 h), the PL blueshifts from 1.51 to 1.7 eV, accompanied by a decrease in the intensity. This indicates that upon annealing at 400 °C, the growth rates of PL centers are much faster than their decay rates. Similar to the cases for 500 and 600 °C annealing, we see a complete spectral change process also for 400 °C annealing, i.e. a redshift of the peak energy accompanying an increase in PL intensity at short annealing time and a blueshift of the peak energy accompanying a decrease in PL intensity at long annealing time. For the case of 400 °C annealing, the final thermodynamic stable PL is also the PL approximately 1.75 eV.

3.5. Kinetic oscillations of the red PL upon 400 °C annealing

It was found that upon 400 °C annealing, during the decay process of the PL centers (blueshift of the PL), a short time annealing causes the recovery of the PL centers (re-redshift of the PL). This leads to the spectral shift and the peak intensity vs. accumulation annealing times show temporal oscillations as shown in Fig. 11. The sample shows a weak PL approximately 1.75 eV before 400 °C annealing. With increasing annealing times ($<$10 h), the PL gradually redshifts from 1.75 to 1.46 eV and its intensity increases by a factor of 18. A

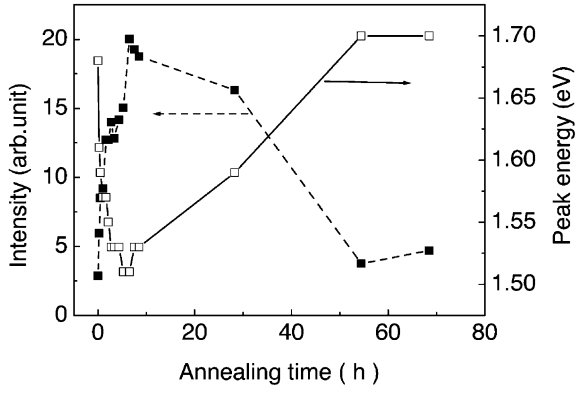

Fig. 10. The dependence of the peak energy (solid square + dash line) and the PL intensity (open square + solid line) on annealing times upon 400 °C FG annealing.

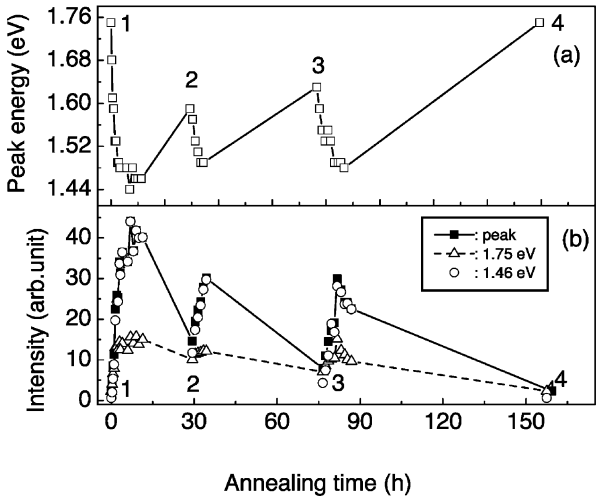

Fig. 11. The peak energy (a) and the PL intensities at 1.75 eV, at 1.46 eV, and at the peak energy (b) vs. annealing times for 400 °C annealing temperature. A demonstration of the temporal oscillation.

subsequent 18 h annealing blueshifts the PL from 1.46 to 1.59 eV and reduces its intensity by a factor of 2.8. From this position, annealing at shorter times (<5 h) leads to a redshift from 1.59 to 1.49 eV and to an increase in the intensity while annealing at longer times (42 h) results in a blueshift from 1.49 to 1.63 eV and in a decrease of the intensity. From 1.63 eV, again at shorter times (<8 h), the PL redshifts from 1.63 to 1.49 eV with a 3.5 times increase in the intensity, whereas at longer times (70 h), it blueshifts from 1.49 to 1.75 eV with an 11 times decrease in the intensity. From Fig. 11, we obtain the following important results: (1) it reproduces the 400 °C annealing behaviors we observed above for other samples (for example in Fig. 10), i.e. a short time growth process and a long time decay process. (2) During the decay process of PL centers, the PL centers can recover using a short annealing time. This makes the spectral shift and the intensity variation versus accumulation annealing times exhibit temporal oscillatory behavior. Each oscillation is composed of two time segments, i.e. a shorter time segment with a redshift in the peak energy and an increase in intensity and a longer time segment with a blueshift in the peak energy and a decrease in intensity. In addition, the increase in intensity and the degree of redshift decrease with cycling times. (3) As shown in Fig. 11b point 1 (1.75 eV), 2 (1.59 eV), and 3 (1.63 eV), the growth of PL centers can be initiated at different peak energies during the decay process of the PL centers. This leads to an aperiodic oscillatory behavior. Therefore the oscillatory behavior is a pure kinetic one.

From III B to D, we have already found that there exist two PL centers in the red PL. One is approximately 1.5 eV and the other is approximately 1.75 eV. The actual PL is composed of both. The difference in their formation and decay kinetics leads to the observed spectral change for the PL. Therefore, in Fig. 11b, apart from the PL intensity at peak energy, we also exhibit the PL intensities at 1.75 and 1.46 eV with annealing time. We can see that the growth rate of 1.46 eV PL centers is faster than that of 1.75 eV PL centers. This difference in the growth rates for these two PL centers leads to the redshift of the PL. After the concentrations of PL centers reach maximum, the growth process can be neglected and the decay process of PL centers dominates. The decay rate for 1.46 eV PL is faster than that for 1.75 eV. This difference in the decay rates results in the blueshift of the PL. We also notice that for 1.75 eV PL and 1.46 eV PL, their growth rates are much larger than their decay rates. As seen from Figs. 10 and 11, we know that the PL approximately 1.75 eV is the final thermodynamic stable state and that the PL approximately 1.5 eV is a metastable state for 400° annealing. The existence of this metastable state is one of the reasons that we can observe the oscillatory behavior. At this metastable state, the concentration of PL centers reaches its maximum (at least for the 1.5 eV PL centers). During the slow decay process, the system deviates from this metastable state and therefore produces a driving force to go back. Due to the fast growth rates of the PL centers, we observe their recovery at short annealing time.

4. Discussion

4.1. The source of the red PL

As outlined in Section 1, two sources are suggested to be the origin of the visible PL in PS and in nc-Si. One is nc-Si itself. Another is interfacial defect state. If the PL is from nc-Si, according to the pure QSE model, the PL approximately 1.5 eV should be mainly due to the larger nc-Si while the PL approximately 1.75 eV should be mainly due to the smaller nc-Si. Then the continuous redshift of the PL from 1.75 to 1.5 eV should correspond to the gradual increasing in the average grain size (assuming a Gaussian size distribution). If this is the case, with the gradual increasing in the PL intensity approximately 1.5 eV, the PL intensity approximately 1.75 eV should correspondingly decrease since some of smaller particles become larger particles. The blueshift of the PL should be the other way round. However, the experimental results indicate that during the redshift of peak energy from 1.75 to 1.5 eV, with the gradual increasing in the PL intensity approximately 1.5 eV, the PL intensity approximately 1.75 eV also increases. This therefore repulses the idea that the distribution of grain size changes. In addition, XRD diagrams show no observable change after low temperature annealing, indicating no variations in the nc-Si size and amount. (2) The spectral oscillation upon 400 °C annealing indicates

that this oscillation is a pure kinetic one. It can be initiated at different peak energies during the decay process of the PL centers. It rules out the structural phase transition or the size variation of nc-Si itself as the oscillatory element. Our results therefore exclude nc-Si itself as the source of the red PL in our case. As a result, the source of the red PL should be defect-state-related PL centers.

As mentioned above, our earlier defect studies using ESR technique have already built up the correlation between the intensity of PL approximately 1.5 eV and the concentration of oxygen TDs-like defect state [23]. It is known that oxygen TDs widely exist in oxygen-enriched crystalline silicon under low temperature annealing (300–550 °C) [30–32]. Up to now, 17 TD species ($(TD)_n$, $1 \leqslant n \leqslant 17$) have been identified, which develop sequentially upon heat treatment with the more shallow species being generated later [33]. From ESR measurements, individual $(TD)_n$ cannot be distinguished, and mainly two signals (Si-NL8 state and Si-NL10 state) are related to oxygen TDs. The main features of these two oxygen TDs can be summarized as follows: (1) the formation process of Si-NL8 state is normally faster than that of Si-NL10 state. Si-NL8 state is less stable at long annealing times and at higher temperatures compared to Si-NL10 state [34]. (2) The concentration of oxygen TDs in crystalline Si from ESR measurements upon low temperature annealing first increases with annealing time, then reaches a maximum, and finally decreases [34]. (3) The important factors that control the formation of TDs are the annealing temperature and annealing time. Detailed studies show that at temperatures below 450 °C the formation rate is decreased and the saturation concentration of TDs is less than that for a 450 °C thermal treatment. Above 450 °C the saturation concentration of TDs decreases with increasing temperature [35].

The effect of isochronal annealing (60 min) at different temperatures on the PL intensities at 1.75 and 1.46 eV is given in Fig. 12. Here the temperature range for the increase of the PL intensity further shows a correlation with the formation temperature range of oxygen TDs in crystalline Si, over the temperature range 300–550 °C. As shown in Fig. 7a and b, for annealing temperatures between 300 and 500 °C the PL intensity approximately 1.46 eV increases much faster than the PL intensity approximately 1.75 eV whereas above 400 °C the former annihilates much faster than the latter. In addition, for 500 and 600 °C annealing, the PL intensities at 1.75 and 1.46 eV vs. annealing times show a process of increasing, reaching maximum, then decreasing, similar to the annealing behavior of Si-NL8 state and Si-NL10 state [34]. Comparing the above features of the PL centers with those of oxygen TDs, we can further postulate that the PL approximately 1.75 eV is mainly due to Si-NL10-like defect states while the PL

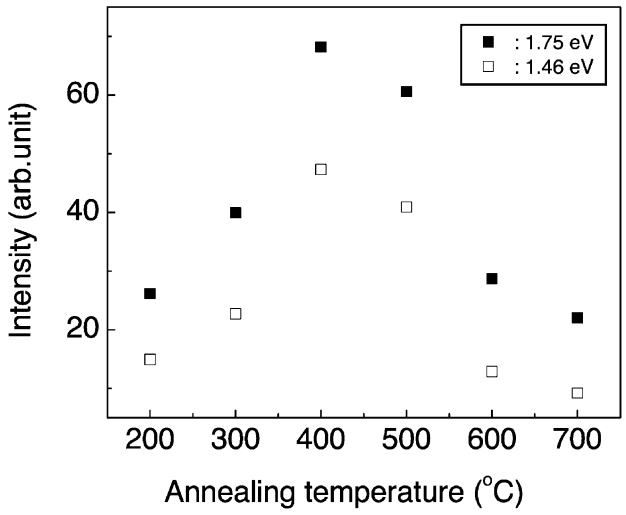

Fig. 12. Isochronal annealing curve for PL intensities at 1.75 and 1.46 eV. The duration of the annealing time was 60 min at each temperature.

approximately 1.5 eV is composed of both Si-NL8- and Si-NL10-like defect states and is dominated by Si-NL8 states. The red PL consists of these two states. The peak energy and the PL intensity are determined by the concentrations of these two components at the corresponding annealing temperature and time.

4.2. The annealing conditions dependence of the red PL

Now we can explain the spectral change of the PL from 1.75 to 1.5 eV. For a PL approximately 1.75 eV, upon annealing at lower temperatures (<600 °C), first both Si-NL8- and Si-NL10-like states grow, but the former forms much faster, and thus the PL redshifts and the intensity increases. When the concentration of Si-NL8-like state reaches its maximum, the redshift and the increase in the PL intensity also reach a maximum. Upon further annealing, both states gradually decay. Since Si-NL8-like states decay faster than Si-NL10-like states, the PL gradually blueshifts and the PL intensity also decreases. Finally, only Si-NL10-like states exist and show a PL approximately 1.75 eV. For lower annealing temperatures (<400 °C), due to the lower formation rate, the whole annealing period corresponds to the growth process of PL centers. For intermediate temperatures (400–600 °C), we observe a complete growth, saturation and decay process. From Fig. 6, we can also see that the degree of the redshift in the peak energy and the magnitude of the increase in the integrated PL intensity decrease with increasing annealing temperatures from 400 to 600 °C. This is again due to the difference in the growth and decay kinetics of these two states. With increasing annealing temperatures from 400 to 600 °C, the growth rates for Si-NL8- and Si-

NL10-like states both increase, but the former increases less than the latter (Fig. 7). This causes the difference in the growth rates of these two states decreasing with increasing temperatures. Therefore, the degree of the redshift in the peak energy also decreases with increasing annealing temperature. On the other hand, with increasing annealing temperatures, the decay rates for these two states also increase very fast. This leads to the saturation concentration of these two states decreasing with increasing temperatures, which agrees with the dependence of saturation concentration for oxygen TDs in bulk Si on annealing temperatures [35]. This explains the magnitude of increase in the PL intensity decreasing with increasing annealing temperature from 400 to 600 °C.

The unique dependence of PL intensities on PL energies (Fig. 6) can also be explained. Since the redshift of PL energies corresponds to the growth process of PL centers, the PL intensities naturally increase with the redshift of PL energies. Upon annealing at 400 °C under FG atmosphere, the spectral shift and the peak intensity vs. annealing times show a kinetic oscillatory behavior. In a closed system, the concentrations, which vary in an oscillatory way, are those of the intermediates [36]. As already discussed above, both Si-NL8 state and Si-NL10 state are intermediates. Therefore they satisfy one of the conditions for oscillations in a closed system. However, the detailed mechanism for this spectral oscillation is unclear now.

4.3. Comparison with aged or oxidized PS

For oxygen-passivated Si clusters or aged PS, depending on the size of the cluster, three recombination mechanisms have been suggested by Wolkin et al. [18]. In large size, recombination is via free excitons since the band gap is not wide enough to stabilize the Si=O surface state. In medium size, recombination involves a trapped electron and a free hole. As the size decreases, the PL emission energy still increases, but not as fast as predicted by quantum confinement, since the trapped electron state energy is size independent. In quite small size (<2 nm), recombination is via trapped excitons (Si=O surface state). As the size decreases, the PL energy stays constant, and there is a large PL redshift when nanocrystallite surface becomes exposed to oxygen. In our case, the spectral change from 1.3 to 1.55 eV (Fig. 1b–d) is similar to the case of medium size suggested by Wolkin et al. since the blueshift of the PL accompanies the decrease of the nc-Si size (Fig. 2b–d). However, due to the coexistence of two PL centers, the explanation of spectral change is much more complicated. The spectral change from 1.5 to 1.75 eV corresponds to the case of quite small size, i.e. recombination is via trapped excitons. However, in our case, the PL energy does not stay constant due to the coexistence of two PL centers with different emission energies in one PL and due to their variance in annealing temperature- and time-dependence.

Although Si–O related defect states have been verified to give visible PL in aged and oxidized PS by many groups, the detailed structures of them are unknown [7,11,18,37–39]. The unique dependence of the red PL on annealing conditions in our nc-Si/SiO_2 films have not been observed in aged and oxidized PS. We believe that the key structure of Si–O related defect states that gives visible PL with several tens of microseconds decay at room temperature should be similar. However, the detailed structures of them may be different due to different preparation methods and conditions. This will lead to some specific PL features as we observed here for our nc-Si/SiO_2 films. Despite much more knowledge of oxygen TDs-like defect states, we do not know the structural details of them due to the following two reasons. Although much research has been done on oxygen TDs in bulk crystalline Si, their core structures and formation mechanism are still unclear [35]. Owing to the complex structure of the nc-Si/SiO_2 film, the formation and annihilation as well as the configuration of oxygen TDs in this system undoubtedly are much more complicated than those in bulk crystalline Si.

5. Conclusion

Experimental results indicate that annealing conditions during the post-treatment process play a central role in the spectral change of the red PL. The main results are summarized as follows:

(1) The spectral change between 1.75 and 1.5 eV upon FG annealing shows a strong correlation with the annealing behavior of oxygen TDs. The PL approximately 1.75 eV is mainly due to Si-NL10-like defect states while the PL approximately 1.5 eV comes from both Si-NL8- and Si-NL10-like defect states. According to their variance in annealing temperature- and time-dependence, the emission energy can be tuned from 1.75 to 1.5 eV.

(2) FG annealing is very important for the enhancement of the red PL by effectively decreasing the density of nonradiative recombination centers.

(3) The red PL is composed of Si-NL8 and Si-NL10-like defect states. The peak energy and the spectral shape are determined by the concentration ratio of these two components while the PL intensity is determined by the concentrations of these two components and the density of nonradiative recombination centers. The increase of the PL intensity versus the redshift of the peak energy reflects the formation process of two PL centers.

(4) For a PL approximately 1.75 eV, upon annealing at 400 °C in FG atmosphere, the spectral shift and the

peak intensity versus annealing times show a temporal oscillation. This oscillation is a pure kinetic one.

(5) The dependence of spectral change from 1.75 to 1.5 eV on annealing conditions and the temporal oscillation of the spectral change upon annealing at 400 °C repulse nc-Si itself as the source of the red PL, however favor oxygen TDs-like defect states instead.

In conclusion, present study not only adds more evidence that oxygen TDs-like defect state is the source of the red PL, but also further distinguishes two PL centers in this red PL. The mechanism of the spectral oscillations and the structures of oxygen TDs-like defect states in nc-Si/SiO_2 films need further investigation.

Acknowledgments

X.C. Wu acknowledges financial support from the Alexander von Humboldt Foundation.

References

[1] L.T. Canham, Appl. Phys. Lett. 57 (1990) 1046.
[2] Y. Kanemitsu, Phys. Rep. 263 (1995) 1.
[3] A.G. Cullis, L.T. Canham, P.D.J. Calcott, J. Appl. Phys. 82 (1997) 909.
[4] A.G. Cullis, L.T. Canham, Nature 353 (1991) 335.
[5] F. Koch, V. Petrova-Koch, T. Muschik, A. Nikolov, V. Gavrilenko, Mater. Res. Soc. Symp. Proc. 283 (1992) 197.
[6] S.M. Brant, D.H. Fuchs, M. Stutzmann, J. Weber, M. Cardona, Solid State Comm. 81 (1992) 307.
[7] M.S. Prokes, J.U. Glembocki, U.M. Bermudez, R. Kaplan, E.L. Friedersdorf, C.P. Searon, Phys. Rev. B 45 (1992) 13788.
[8] C. Tsai, H.K. Li, S.D. Kinosky, Z.R. Qian, C.T. Hsu, T.J. Irby, S.K. Banerjee, K.B. Hance, M. White, J. Appl. Phys. Lett. 60 (1992) 1700.
[9] S. Veprek, M. Ruckschloss, B. Landkammer, O. Ambacher, Mat. Res. Soc. Symp. Proc. 298 (1993) 117.
[10] M.S. Proke, Appl. Phys. Lett. 62 (1993) 3244.
[11] J.L. Gole, D.A. Dixon, J. Phys. Chem. B 101 (1997) 8098.
[12] J.L. Gole, F.P. Dudel, D. Grantier, D.A. Dixon, Phys. Rev. B 56 (1997) 2137.
[13] J.L. Gole, D.A. Dixon, J. Phys. Chem. B 102 (1998) 1768.
[14] Y. Kanemitsu, T. Ogawa, K. Shiraishi, K. Takeda, Phys. Rev. B 48 (1993) 4883.
[15] T. Wadayama, T. Arigane, A. Hatta, Appl. Phys. Lett. 73 (1998) 2570.
[16] D.W. Cooke, B.L. Bennett, E.H. Farnum, W.L. Hults, K.E. Sickafus, J.F. Smith, J.L. Smith, T.N. Taylor, P. Tiwari, A.M. Portis, Appl. Phys. Lett. 68 (1996) 1663.
[17] K.O. Andersen, E. Veje, Phys. Rev. B 53 (1996) 15643.
[18] M.V. Wolkin, J. Jorne, P.M. Fauchet, G. Allan, C. Delerue, Phys. Rev. Lett. 82 (1999) 197.
[19] H. Takagi, H. Ogawa, Y. Yamazaki, A. Ishizaki, T. Nakagiri, Appl. Phys. Lett. 24 (1990) 2379.
[20] T. Ito, T. Ohta, A. Hiraki, Jpn J. Appl. Phys. 31 (1992) L1.
[21] M.L. Brongersma, A. Polman, K.S. Min, E. Boer, T. Tambo, H.A. Atwater, Appl. Phys. Lett. 72 (1998) 2577.
[22] S. Veprek, Th. Wirschem, in: R.E. Hummel, P. Wissmann (Eds.), Handbook of Optical Properties, vol. 2, CRC Press, Boca Raton, 1997, p. 129.
[23] S.M. Prokes, W.E. Carlos, S. Veprek, Ch. Ossadnik, Phys. Rev. B 58 (1998) 15632.
[24] X.C. Wu, Ch. Ossadnik, Ch. Eggs, S. Veprek, F. Phillip, J. Vas. Sci. Technol. B 20 (2002) 1368.
[25] S. Shin, K.H. Jung, J. Yan, D.L. Kwong, M. Kovar, J.M. White, Appl. Phys. Lett. 63 (1993) 3306.
[26] P. Czaputa, R. Fritzl, A. Popitsch, Thin Solid Films 255 (1995) 212.
[27] R.T. Collins, M.A. Tischler, J.H. Stathis, Appl. Phys. Lett. 61 (1992) 1649.
[28] L. Tsybeskov, P.M. Fauchet, Appl. Phys. Lett. 64 (1994) 1983.
[29] D.W. Cooke, B.L. Bennett, E.H. Farnum, W.L. Hults, K.E. Sickafus, J.F. Smith, J.L. Smith, T.N. Taylor, P. Tiwari, A.M. Portis, Appl. Phys. Lett. 68 (1996) 1663.
[30] T. Gregorkiewicz, H.H.P.Th. Bekman, C.A.J. Ammerlaan, Phys. Rev. B 41 (1990) 12628.
[31] W. Goetz, G. Pensl, Phys. Rev. B 46 (1992) 4312.
[32] P. Deak, L.C. Snyder, J.W. Corbett, Phys. Rev. B 45 (1992) 11612.
[33] C.A.J. Ammerlaan, I.S. Zevenbergen, Yu.V. Martynov, T. Gregorkiewicz, in: R. Jones (Ed.), Early Stages of Oxygen Precipitation in Silicon, Kluwer Academic Publishers, Dordrecht, 1996, p. 61.
[34] T. Gregorkiewicz, D.A. van Wezep, H.H.P.Th. Bekman, C.A.J. Ammerlaan, Phys. Rev. B 35 (1987) 3810.
[35] J. Michel, L.C. Kimerling, in: F. Shimura (Ed.), Oxygen in Silicon, Academic Press, San Diego, CA, 1994, p. 251.
[36] P. Gray, S.K. Scott, Chemical Oscillations and Instabilities, Clarendon Press, Oxford, 1990.
[37] I. Coulthard, W.J. Antel, J.W. Freeland Jr., T.K. Sham, S.J. Naftel, P. Zhang, Appl. Phys. Lett. 77 (2000) 498.
[38] J.P. Wang, L. Song, B.S. Zou, M.A. El-Sayed, Phys. Rev. B 59 (1999) 5026.
[39] H.E. Porteanu, E. Lifshitz, Th. Dittrich, V. Petrova-Koch, Phys. Rev. B 60 (1999) 15538.